Growth and characterisation of MnSb(0001)/InGaAs(111)A epitaxial films

P.J. Mousley[1] , C.W. Burrows[1], M.J. Ashwin[1], A.M. Sánchez[1], V.K. Lazarov[2] and G.R. Bell[1]

[1] *Department of Physics, University of Warwick, Coventry CV4 7AL, UK*

[2] *Department of Physics, University of York, York YO10 5DD, UK*

Abstract

MnSb layers have been grown on $In_xGa_{1-x}As$(111)A virtual substrates using molecular beam epitaxy (MBE). The effects of both substrate temperature (T_{sub}) and Sb/Mn beam flux ratio ($J_{Sb/Mn}$) were investigated. The surface morphology, layer and interface structural quality, and magnetic properties have been studied for a 3×3 grid of T_{sub} and $J_{Sb/Mn}$ values. Compared to known optimal MBE conditions for MnSb/GaAs(111) [T_{sub}=415 °C, $J_{Sb/Mn}$=6.5], a lower substrate temperature is required for sharp interface formation when growing MnSb on $In_{0.48}Ga_{0.52}As$(111)A [T_{sub}=350 °C, $J_{Sb/Mn}$=6.5]. At high flux ratio ($J_{Sb/Mn}$=9.5) elemental Sb is readily incorporated into MnSb films. At higher substrate temperatures and lower flux ratios, (In,Ga)Sb inclusions in the MnSb are formed, as well as MnAs inclusions within the substrate. The Sb and (In,Ga)Sb inclusions are epitaxial, while MnAs inclusions are endotaxial, i.e. all have a crytallographic relationship to the substrate and epilayer. MBE optimisation towards different device structures is discussed along with results from a two-stage growth scheme.

Keywords: A3. Molecular beam epitaxy, B1. MnSb, B2. Half-metallic ferromagnet, B1. InGaAs

1. Introduction

The epitaxial combination of magnetic and semiconducting materials can underpin new spintronic device technologies with great potential for low-energy computation and data storage [1]. Two canonical spintronic devices

are the spin valve and the spin field-effect transistor. For the latter in particular, $In_xGa_{1-x}As$ conducting channels are attractive, this material having high electron mobility and electron g-factor [2, 3]. Transition metal monopnictides are materials that may be ideal for spintronic applications in combination with III-V semiconductor structures since they can be grown epitaxially by conventional molecular beam epitaxy (MBE) and have a wide variety of controllable magnetic properties.

Examples of transition metal monopnictide epitaxial growth on GaAs substrates include MnAs [4, 5, 6], CrAs [7], MnSb [8, 9, 10] and NiSb [11]. Compared to GaAs, rather fewer MBE growth studies have been carried out on $In_xGa_{1-x}As$ or related substrates. Amemiya et al. grew MnSb on an InGaAsP-based structure to fabricate a high-performance optical waveguide isolator [12]. Earul Islam and Akibori grew MnAs on InAs(111)B virtual substrates (grown on GaAs) [13] and fabricated a lateral spin valve showing a room temperature spin injection efficiency of approximately 8.5% and spin diffusion length of 0.7 μm [14]. Oomae et al. grew MnAs directly on InP, with the presence of the fully spin-polarized cubic B3 polymorph reported [15]. MnSb has been grown on $In_xGa_{1-x}As$ virtual substrates [16], a system for which a good lattice match can be achieved, and co-existence of cubic and hexagonal MnSb polymorphs was shown.

MnSb is a ferromagnetic material with high Curie temperature (589 K) which can be grown by MBE on a variety of semiconductor substrates [17] [18] [19]. The cubic B3 polymorph of MnSb is predicted to have robust half-metallicity (100% spin polarization at the Fermi level) even at room temperature [8], with high spin polarisation retained at III-V interfaces [20]. The stable hexagonal $B8_1$ polymorph (niccolite structure) is predicted to have enhanced spin polarisation at III-V interfaces [21]. In all cases the electrical conductivity is much lower than typical 3d transition metals, which can help to alleviate the well-known conductivity mismatch problem [22]

Our group has previously investigated the formation of both the niccolite and cubic MnSb polymorphs (n-MnSb and c-MnSb) on $In_xGa_{1-x}As(111)$ virtual substrates [16]. In this paper we present a detailed MBE growth study aimed at gaining a better understanding of this material system. The study explores the parameter space of MBE growth conditions for MnSb on $In_xGa_{1-x}As(111)A$, focussing on substrate temperature and flux ratio $J_{Sb/Mn}$ calculated from beam equivalent pressures (BEP). Characterization was performed using in situ reflection high energy electron diffraction (RHEED), as well as ex situ atomic force microscopy (AFM), scanning electron microscopy

(SEM), scanning transmission electron microscopy with energy dispersive X-ray spectroscopy (STEM and EDX), X-ray diffraction (XRD) and vibrating sample magnetometry (VSM).

2. Experimental details

MnSb layers were grown on $In_xGa_{1-x}As$(111)A virtual substrates, which consist of 400 nm (In,Ga)As(111) on GaAs(111), via co-deposition of Mn and Sb_4. The XRD reported below gives an out-of-plane lattice parameter consistent with a virtual substrate composition of $In_{0.48}Ga_{0.52}As$, neglecting residual epitaxial strain. Virtual substrate growth has been detailed previously [16]. The fixed Mn flux and deposition time correspond to approximately 120 nm thick MnSb films grown at 2 nm / min. and growth was initiated by opening Mn and Sb cells simultaneously. A 3×3 grid of substrate temperatures (T_{sub} = 350, 415, 450 °C) and flux ratios ($J_{Sb/Mn}$ = 3.5, 6.5, 9.5) was investigated. All samples were grown using a dedicated home-built MBE system which has shuttered Mn and Sb effusion cells, a retractable beam flux gauge and an electron gun with phosphor screen to allow in situ RHEED measurements (beam energy 12.5 keV). The Sb cell had no cracker stage and no As cell was fitted.

$In_{0.48}Ga_{0.52}As$(111)A samples approximately 8 mm × 8 mm were mounted onto stainless steel sample plates using spot-welded tantalum wires. These were ultrasonicated and rinsed with a series of solvent washes (acetone, isopropanol, and then deionised water). After cleaning the samples were blown dry with nitrogen and loaded immediately into the MBE vacuum system. Once transferred into the preparation chamber all of the samples were cleaned by annealing at 425 °C for 1 hour, followed by argon ion bombardment for 8 minutes at 500 eV, and then annealing at 490 °C for 1 hour. Argon ion sputtering and annealing may produce both enhanced n-type doping near the $In_{0.48}Ga_{0.52}As$ surface [23] and metallic In/Ga clusters [16, 24]. The possible effects of metal clusters on MnSb MBE growth will be discussed later, while electrical transport measurements will be reported in a future paper.

A full sample set across the 3×3 grid of growth conditions was grown using a single-stage growth methodology, where the substrate temperature was held constant throughout MnSb deposition. The T_{sub}= 415°C growth conditions were also conducted using a two-stage growth methodology, where an initial co-deposition step was carried out for 60 seconds at T_{sub} = 350°C,

and then the growth was interrupted while the substrate was heated to T_{sub}= 415°C to be held at this temperature for the remainder of the growth.

3. Results

3.1. RHEED

The surface preparation procedure for the virtual substrates produced an ordered $In_{0.48}Ga_{0.52}As$(111)A surface with (2×2) periodicity. We did not attempt to determine this reconstruction quantitatively, but it is most likely a "missing Ga(In)" structure by comparison to the (2×2) found both on GaAs(111)A [25] and InAs(111)A surfaces [26]. A small selection of example RHEED patterns obtained after MnSb layer growth is shown in figure 1, with the lower section showing example patterns of the individual features. Examples along both principal surface azimuths are shown, namely $\langle 11\bar{2}0\rangle$ [A and C, both showing (1×1) periodicity] and $\langle 10\bar{1}0\rangle$ [E and D, both showing (2×2) periodicity]. A sharp (2×2) periodicity with higher Laue zones and Kikuchi features was present for all samples grown with $J_{Sb/Mn}$= 6.5. Previous work on $B8_1$ structured MnSb(0001) has shown that this surface reconstruction is associated with smooth and well-ordered MnSb surfaces [27] [28]. For $J_{Sb/Mn}$= 6.5 samples grown with $T_{sub} \geq$ 415°C, very faint incommensurate transmission spots were present (example E). Their spacing in the RHEED pattern corresponds to a material with an in-plane lattice parameter of 4.54 Å, approximately 10% larger than n-MnSb.

The use of the high flux ratio $J_{Sb/Mn} = 9.5$ formed a (1×1) surface reconstruction occasionally showing very faint fractional-order streaks. Transmission spots commensurate with the integer order surface streaks were present for growth at T_{sub} = 350°C and 415°C, but these were absent for two-stage growth and for T_{sub} = 450°C (example C). Only the lowest-order Laue zone was present in the RHEED patterns, and Kikuchi lines were not present, for the low growth temperature of T_{sub} = 350°C at $J_{Sb/Mn} = 9.5$ (example A). For MBE growth conditions using a low flux ratio of $J_{Sb/Mn} = 3.5$ the RHEED patterns became very weak, with the higher temperatures $T_{sub} \geq$ 415°C producing only faint and modulated streaks. Neither higher Laue zones nor Kikuchi lines were present in RHEED patterns from any single-stage MnSb layers grown at $J_{Sb/Mn} = 3.5$. The two-stage growth produced a slight improvement, with a (2×2) periodicity present alongside incommensurate transmission spots. Overall, RHEED patterns of the best quality were observed

for $J_{Sb/Mn} = 6.5$. We now turn to ex situ measurements to understand this behavior in more detail.

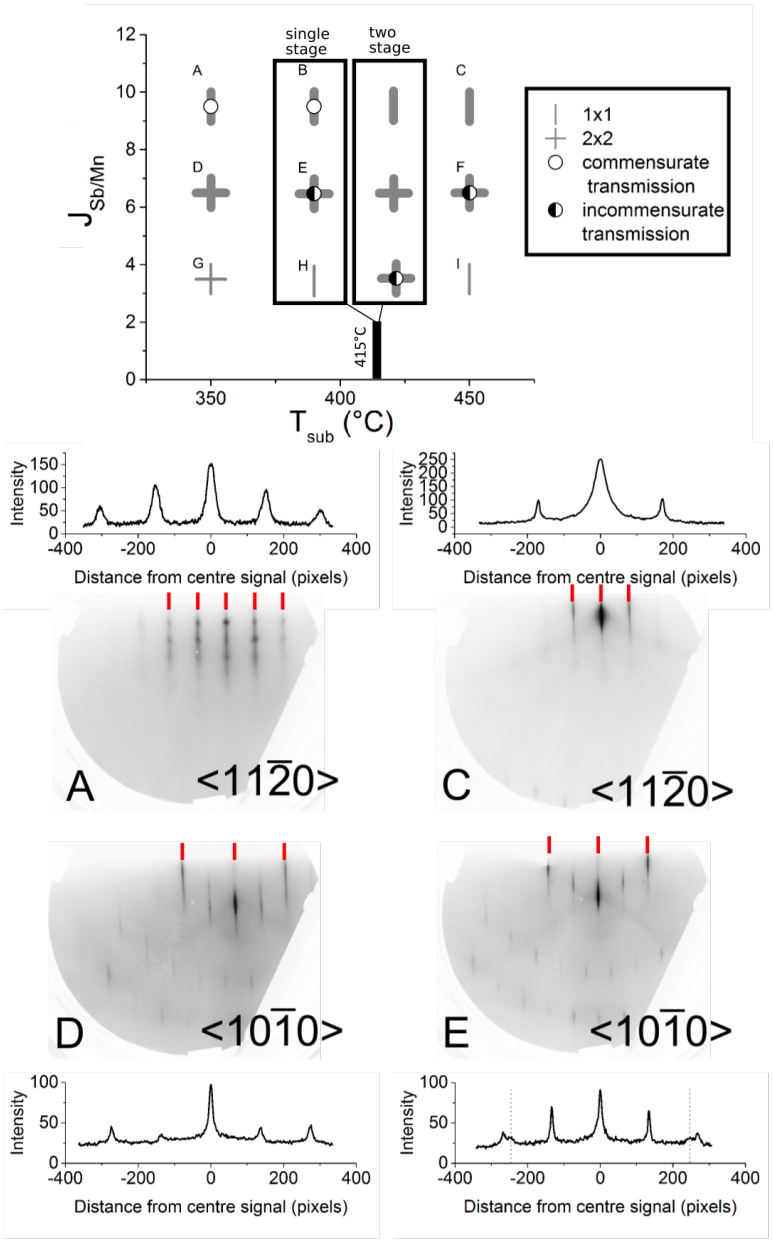

Figure 1: RHEED pattern summary (upper panel) and examples (lower panels) for MnSb growth on InGaAs(111)A as a function of substrate temperature T_{sub} and Sb/Mn flux ratio $J_{Sb/Mn}$. Patterns A,C,D and E exemplify the main features observed in the two principal surface azimuths, and line profiles across each pattern are also shown. Red lines indicate the integer streak positions for each pattern.

3.2. SEM and AFM

Imaging by SEM at low magnification showed clearly that crystallites ranging between 0.1 μm and 1 μm in diameter were formed on the surface during growth for all samples. Example crystallites are circled in red (figure 2a). The vertical extent of individual crystallites increased with higher $J_{Sb/Mn}$, which suggests that the crystallites are capturing excess Sb and are therefore likely formed of $MnSb_2$ or Sb. They appear too large to contribute to transmission diffraction in RHEED, and not flat enough to contribute to surface diffraction, and so probably act to increase the diffuse background in the patterns. The areal surface densities of these crystallites measured from each growth condition, for both single-stage and two-stage growth methodology, are shown in figure 2b (error bars estimated assuming Poisson statistics). This analysis shows that $J_{Sb/Mn} = 6.5$ leads to higher quality surfaces with fewer crystallites forming, and that these areal densities are decreased using a two-stage growth method.

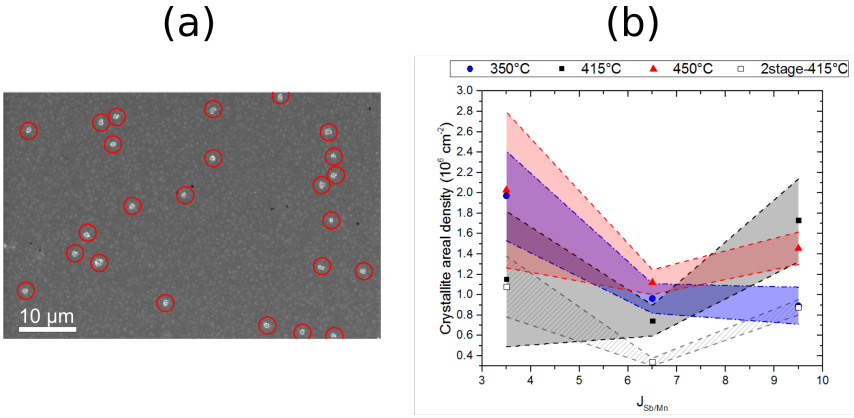

Figure 2: (a) An example SEM image with surface crystallites circled in red (b) areal densities of crystallites for all growth conditions. Shaded regions represent the error bars due to counting statistics.

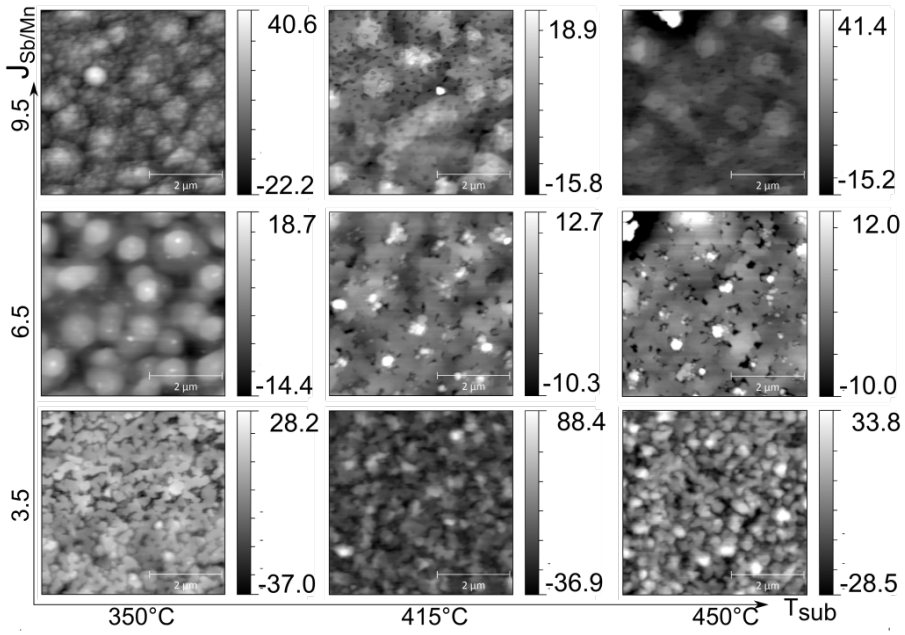

Figure 3: AFM topographs (5μm $\times$ 5μm) collected from single-stage growth samples over all growth conditions.

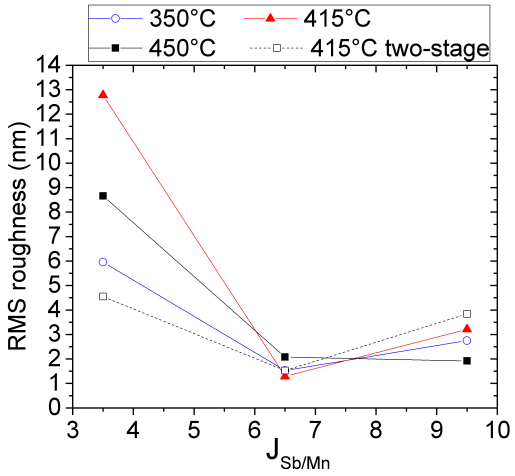

Figure 4: RMS roughness values for single-stage and two-stage samples for all growth conditions, calculated from 1 μm $\times$1 μm AFM images

Example AFM images are shown in figure 3. Samples grown using either the single-stage or two-stage method exhibit similar trends in surface morphology and only single-stage are shown for clarity. At flux ratios $J_{Sb/Mn} \geq 6.5$ some step-terrace structure can be observed, a broadly isotropic mesa-like pattern. Additional islands and pits can be observed, especially at higher temperatures for $J_{Sb/Mn} = 6.5$. These island features are much smaller and higher density than the crystallites observed by SEM and are good candidates for transmission diffraction in RHEED. The crystalline film structure is clearest for $J_{Sb/Mn} = 6.5$ and $T_{sub} = 350°C$, where hexagonal mesas are formed on the surface which are approximately 400 nm in width and 10–15 nm in height. The edges of the hexagonal features show good mutual alignment indicating that these structures are epitaxially related to the substrate. All films deposited using $J_{Sb/Mn} = 3.5$ showed a more disrupted surface with much higher peak-to-peak heights. Both pits and islands are more prevalent and no clear hexagonal structure is observed.

Root mean square (RMS) roughness values calculated from $1\mu m \times 1\mu m$ images for these growth conditions are summarised in figure 4. The surfaces were much rougher for Sb-poor growth with $J_{Sb/Mn} = 3.5$ due to the high density of pits and islands. Under Sb-rich conditions, $J_{Sb/Mn} = 9.5$, roughness was dominated by the hexagonal mesa-like undulations. Both the single stage and two stage growth method produced films with the lowest RMS values when grown using $J_{Sb/Mn} = 6.5$. The most uniform morphology and lowest RMS roughness was observed for single stage growth using $J_{Sb/Mn} = 6.5$ and $T_{sub} \geq 415°C$, with an RMS roughness value of 1.29 nm. RHEED, AFM and SEM all suggest that $J_{Sb/Mn} = 6.5$ is the optimum flux ratio for smooth and ordered MnSb films. By now considering STEM and EDX we can investigate the internal structure of the films.

3.3. STEM

Examples of STEM and EDX data collected from a representative set of single-stage samples is shown in figures 5 and 6. The result of MnSb growth at high and low $J_{Sb/Mn}$ values is shown in figure 5, non-optimal values according to the discussion so far. For growth at $J_{Sb/Mn} = 3.5$ (figure 5a), the MnSb / $In_{0.48}Ga_{0.52}As$ interface can readily be identified by the sharp boundaries in the Sb and As EDX maps. However, it is clear that there is considerable disruption below the interface due to strong intermixing of the metal species. Mn extends several tens of nm into the substrate, forming MnAs. This seems similar to endotaxial growth of MnSb previously observed

on InP [24], GaP [29] and GaSb [30] substrates. In the other direction, Ga diffuses strongly through the MnSb film and In forms large interfacial clusters, displacing Mn. It therefore appears that $In_xGa_{1-x}Sb$ inclusions are formed within the MnSb layer as well as MnAs due to strong exchange of metal species across the interface. The interfacial behavior is very different for growth at $J_{Sb/Mn} = 9.5$ (figure 5b). The STEM and EDX maps show an abrupt interface for all elements without strong intermixing of the metal species across the interface. There is still some Ga segregation through the MnSb film. However, the high Sb flux leads to the formation of Sb inclusions within the growing MnSb layer. These Sb inclusions do not incorporate any Mn, but do appear to attract some segregated Ga.

STEM from samples grown at $J_{Sb/Mn} = 6.5$ (figure 6) again show sharp interfaces between Sb-containing and As-containing regions. However, there is still intermixing of the metal species. From our STEM imaging, this appears to be mostly suppressed for $T_{sub} = 350°C$ (figure 6a) compared to $T_{sub} = 415°C$ (figure 6b). The formation of $In_xGa_{1-x}Sb$ inclusions which reach the sample surface provides a possible explanation for the incommensurate transmission spots observed in RHEED patterns in the latter case. The estimated cubic lattice constant of $\sqrt{2}(4.54)$= 6.42 Å from RHEED would correspond to $In_{0.84}Ga_{0.16}Sb$. Taken together, the data suggest that at $J_{Sb/Mn} = 6.5$ the optimum substrate temperature for interface sharpness (around $T_{sub} = 350°C$) is lower than that for surface smoothness (around $T_{sub} = 415°C$).

The EDX analysis was quantified for several areas imaged by STEM. An example is given in the left panel of figure 6b and table 1, for the sample grown using $T_{sub} = 415°C$ and $J_{Sb/Mn} = 6.5$. The values of EDX analysis presented in table 1 correspond to the numbered areas in the figure. Area 2 comprises $In_xGa_{1-x}Sb$ with similar In and Ga fraction x, but also with Mn intermixed, while areas 1 and 3 are predominantly MnSb but with Ga intermixed. These areas are all above the nominal epilayer / substrate interface, and show some additional As segregation. Below the interface, areas 4 and 5 are predominantly MnAs containing a significant fraction of Ga. Areas 6 and 7 are close to the nominal $In_{0.48}Ga_{0.52}As$ stoichiometry. These data confirm the strong In-Ga / Mn intermixing taking place at the higher substrate temperatures.

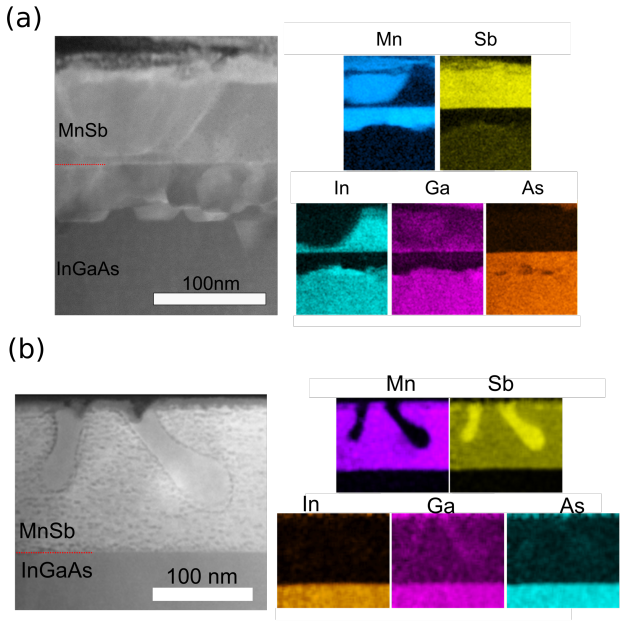

Figure 5: Cross-sectional STEM and accompanying EDX maps taken from samples deposited with (a) $J_{Sb/Mn} = 3.5$ and $T_{sub} = 415°C$ (b) $J_{Sb/Mn} = 9.5$ and $T_{sub} = 350°C$. The color intensity represents the elemental concentration, with black equating to none of the element being present.

Area	Mn%	Ga%	In%		Sb%	As%
1	82	18	0		91	9
2	12	46	42		89	11
3	83	17	0		91	9
4	87	11	2		2	98
5	80	15	6		3	97
6	0	56	44		0	100
7	4	53	43		0	100

Table 1: Compositional analysis for the areas labelled in figure 6b.

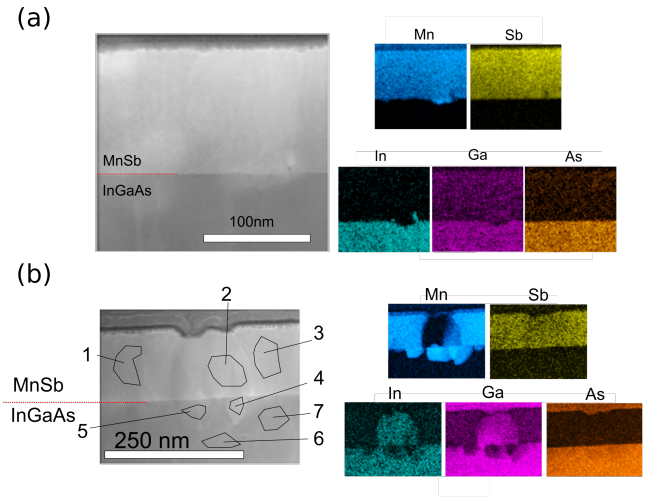

Figure 6: Cross-sectional STEM and accompanying EDX images taken from samples deposited at $J_{Sb/Mn}$ =6.5 with T_{sub} = (a) 350°C and (b) 415°C

3.4. XRD

Having demonstrated the presence of Sb, MnAs and $In_xGa_{1-x}Sb$ in nominally MnSb / $In_{0.48}Ga_{0.52}As$ samples we now examine XRD data to determine if these inclusions are crystallographically aligned. Symmetric out-of-plane $\theta - 2\theta$ XRD scans collected from across the whole 3×3 grid are shown in figure 7. Strong Bragg peaks from the virtual substrate materials are present in all scans. The expected $B8_1$ MnSb(0002) epilayer peak is present in all samples with $J_{Sb/Mn} \geq 6.5$. For single-stage growth at $J_{Sb/Mn}$=3.5 a weak MnSb(0002) feature is present only for T_{sub}=350°C. At higher temperatures for this flux ratio, no MnSb(0002) peak is discernible. However, a clear MnSb($1\bar{1}01$) feature is present. Weaker MnSb($1\bar{1}01$) peaks are observed for the other growth conditions as well; such non-(0001) orientations have been observed for both NiSb and MnSb growth on GaAs(111) [11, 16] but were not previously seen for MnSb on $In_{0.5}Ga_{0.5}As$(111) [16]. The MnSb(0002) peak for samples grown using $J_{Sb/Mn}$ = 9.5 could be fitted with a single Pearson VII function (fits are not shown for clarity), with centroid corresponding to out-of-plane lattice parameters in the range 5.7948 Å to 5.7955 Å. These values are around 0.1% larger than the reported bulk c lattice parameter of 5.789 Å. This may reflect compressive in-plane stress due to Sb inclusions.

In contrast to single-component fits to MnSb(0002) peaks at $J_{Sb/Mn}$ =

9.5, for $J_{Sb/Mn}$=6.5 a minimum of two components was required. The use of two fitting components indicates that there are two distinct out-of-plane strain states of MnSb present for the samples grown at $J_{Sb/Mn} = 6.5$. Note that for T_{sub}=350°C this second strain state appears at higher Q_z (up to -0.4% out-of-plane lattice compression), whereas for $T_{sub} \geq$415°C it appears at lower Q_z (up to +0.6% out-of-plane lattice expansion). This suggests that there are different mechanisms driving the formation of multiple strain states in the MnSb which depend on growth conditions. For $T_{sub} \geq$415°C, the presence of $In_{1-x}Ga_xSb$ within the epilayer may produce local compressive in-plane stress leading to out-of-plane expansion, in a similar manner to the Sb inclusions. However, these explanations remain speculative: selected area electron diffraction may help to elucidate the mechanisms.

All of the single-stage samples show additional peaks at lower Q_z values ($Q_z \leq 1.74$ Å^{-1}). They can be readily assigned to the inclusions observed by STEM-EDX and show that at least a fraction of the inclusions are epitaxially oriented. For samples grown with $J_{Sb/Mn} \leq 6.5$ the low-Q_z features are due to combinations of signals from InSb(111) and $In_xGa_{1-x}Sb$(111). For the single-stage samples with $J_{Sb/Mn} = 9.5$, a clear peak at $Q_z \approx 1.67$ Å^{-1} is assigned to hexagonal Sb(111). For two-stage samples (figure 7b) MnSb(0002) Bragg peaks were present at all $J_{Sb/Mn}$ values. The diffractograms for all three T_{sub} values are identical at $J_{Sb/Mn} = 9.5$ and we would hence expect the two-stage growth at $J_{Sb/Mn} = 9.5$ to look the same. This is indeed the case, with a broad Sb(111) peak appearing at $Q_z \approx 1.67$ Å^{-1} due to epitaxial Sb inclusions. However, the two-stage procedure has clearly not completely suppressed segregation of the metal species from the substrate at $J_{Sb/Mn} \leq 6.5$, since clear $In_xGa_{1-x}Sb$(111) peaks still appear at $Q_z \approx 1.72$ Å^{-1}. The low temperature growth layer is only around 2 nm thick, clearly smaller than the segregation length scales observed by STEM. Nonetheless, the low temperature stage has not introduced detectable Sb inclusions and the two-stage growth process does improve the crystallinity of the MnSb at low flux ratio. The MnSb(0002) peak is much better defined and there is much less evidence of MnAs formation at $J_{Sb/Mn} = 3.5$ compared to the single-stage growths at $T_{sub} = 350$°C and 415°C. This improvement, and the reduced crystallite density (figure 2), may be due to the growth interrupt imposed as part of the two-stage procedure. A longer low-temperature stage and / or a longer growth interrupt may reduce Ga and In segregation without introducing unacceptable Sb inclusion.

The peak observed at $Q_z \approx 2.31$ Å^{-1} for $J_{Sb/Mn}$=3.5 and $T_{sub} = 350$°C

or 415°C, is attributed to $B8_1$ structured MnAs(0002). Together with the STEM-EDX results, this shows that the MnAs formed under these conditions is indeed endotaxial, i.e. crystallographically oriented but below the original substrate surface. Although some MnAs formation is observed by STEM-EDX for $J_{Sb/Mn}$=6.5 (figure 6b) it is clearly either too small in grain size to produce a diffraction feature or is not epitaxial.

3.5. VSM

VSM measurements taken from three representative growth conditions are shown in figure 8 in the form of *M-H* loops. All loops were collected at 10 K, with the applied field aligned in the plane of the sample. The hysteresis loops shown in figure 8a had the diamagnetic response of the substrate removed.

Comparing the 3 samples, it is clear that the sample deposited using $J_{Sb/Mn} = 3.5$ shows significantly degraded magnetic properties (figure 8a), with a much lower overall saturation magnetization and a larger coercieve field. This is consistent with the high degree of disruption of the low-$J_{Sb/Mn}$ films observed and the presence of large non-magnetic inclusions. The two samples grown using $J_{Sb/Mn} = 6.5$ are much more similar in saturation magnetization, as expected, but a closer comparison shows clear differences. The T_{sub}=350°C sample has a lower coerceive field (figure 8b), correlating with the STEM findings which showed it has the lowest level of intermixing in the MnSb layer. This sample also exhibits steps in its *M-H* loop (figure 8c) which is present on both the up and down sweeps of the scan. These steps may be caused by the magnetic switching of hexagonal domains observed in AFM and SEM, where differently sized domains switch magnetic orientation at different applied fields.

Volumes of the MnSb layers were calculated using thickness measurements (obtained from TEM images) along with macroscopic area measurements. These volumes allowed magnetisations per Mn atom to be calculated for all three [T_{sub},$J_{Sb/Mn}$] conditions, assuming the ideal niccolite structure for the whole MnSb layer. The magnetisations of the three films were 1.2 $\pm$0.1μB for [415°C, 3.5], 2.4 $\pm$ 0.2 μB for [415°C, 6.5] and 3.7 $\pm$ 0.4 μB for [350°C, 6.5]. Out of the three samples measured only the growth condition using T_{sub}= 350°C gave a magnetisation in agreement with the published bulk value of 3.5 μB per Mn atom [31]. The low magnetisation per Mn atom for both films grown at 415°C agree with the observations of film intermixing presented earlier. These magnetometry results show that the likely optimum

temperature for thin film magnetic properties may be somewhat lower for MnSb on $In_{0.5}Ga_{0.5}As(111)$ than for MnSb on GaAs(111) (400°C – 420°C).

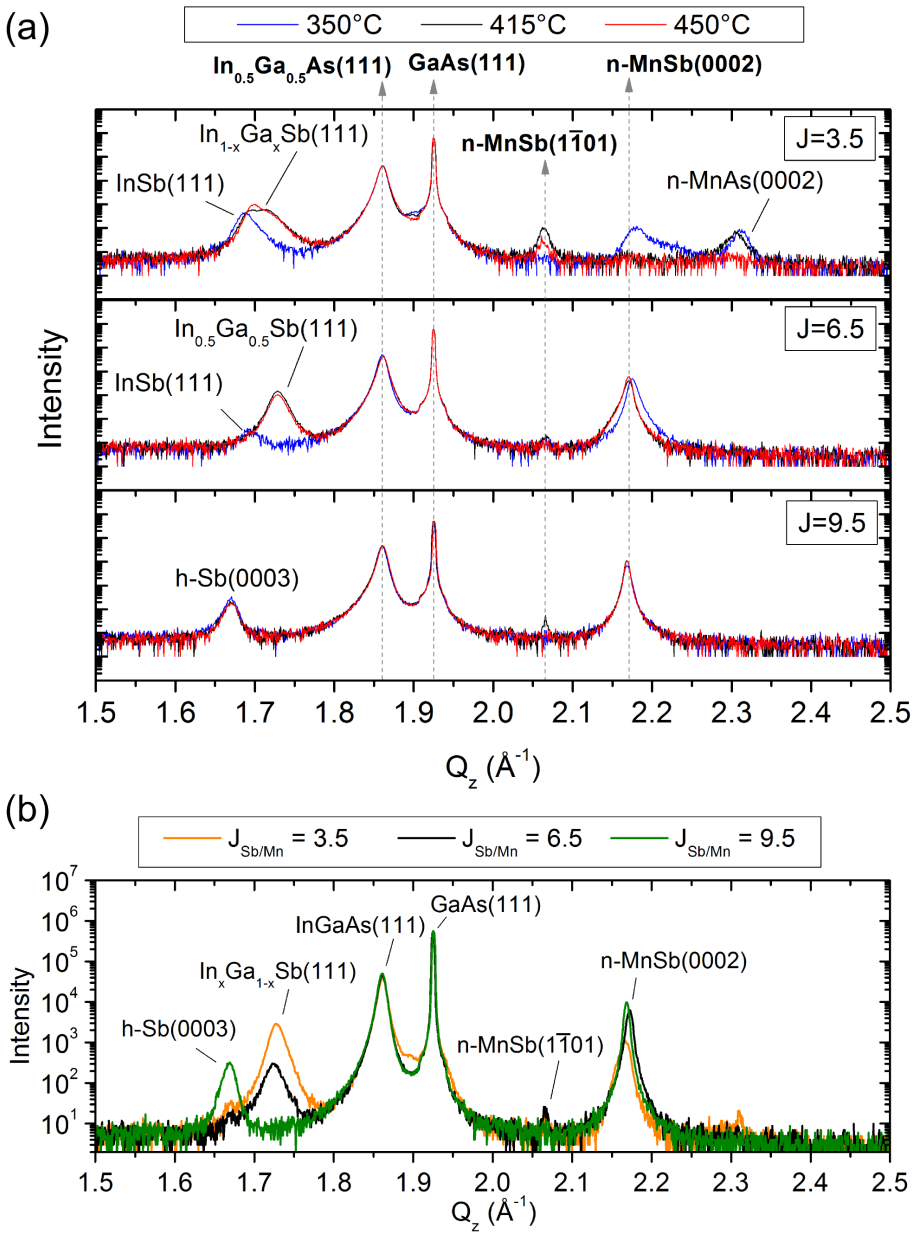

Figure 7: Symmetric X-ray diffraction data for all MnSb samples. Labels h- and n- refer to hexagonal and niccolite structure respectively. (a) XRD from single-stage samples with each panel showing data at different T_{sub} values superimposed for a single value of $J_{Sb/Mn}$. Major peaks found in at least one scan from each $J_{Sb/Mn}$ value are identified by the dotted arrows to bold text at the top of the figure. Other features are labelled individually. (b) XRD data from two-stage samples where data at different T_{sub} values have been superimposed.

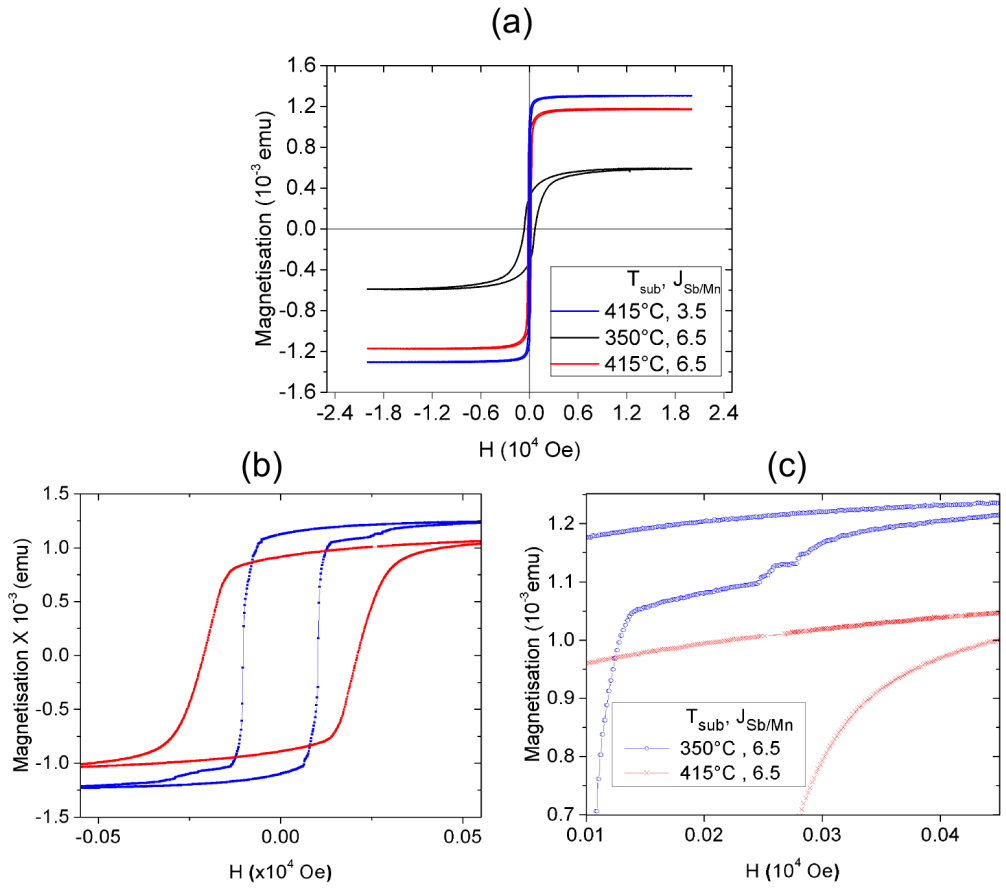

Figure 8: (a) M Vs H measurements obtained using a VSM at 10 K for MnSb/InGaAs(111)A grown using favourable ($J_{Sb/Mn}$=6.5) and non-favourable ($J_{Sb/Mn}$=3.5) growth conditions, with the magnetic field aligned in-plane.(b) and (c) are enlarged versions of the M Vs H loops for $J_{Sb/Mn}$=6.5 samples

4. Discussion and conclusions

An explanation previously suggested for the formation of GaSb inclusions during MnSb / GaAs(111) epitaxy is that surface preparation of the substrate by argon ion sputtering and annealing leaves metallic Ga nano-clusters which readily take up excess Sb during MnSb growth [16, 24]. This does not seem to be applicable here: $In_{0.5}Ga_{0.5}Sb$ growth appears to to be suppressed by high Sb flux which is not what one would not expect if metal droplets were already present on the substrate surface. The In and Ga segregation observed is therefore attributed to diffusion processes, and not to the surface preparation. An important question is whether the metal exchange reaction is thermodynamically favorable. Using estimated enthalpies of formation for Mn(As,Sb) [32] and $In_{0.5}Ga_{0.5}$(As,Sb) [33] the simple exchange reaction has a small energy *cost*: the formation enthalpy of $In_{0.5}Ga_{0.5}As$ + MnSb is -108.9 kJ mol^{-1} while that for $In_{0.5}Ga_{0.5}Sb$ + MnAs is -105.0 kJ mol^{-1}. A simple thermodynamic argument was used to explain trends in surface reactivity for Mn deposition on to different GaAs and InSb reconstructed surfaces [34], but in that case there was no incident group V flux and the temperature was fixed. In the present case the Sb_4 flux clearly has a powerful influence in determining the degree of metal exchange and group V kinetics cannot be neglected. Furthermore both strain and surface energies must surely play a role and a predictive model for endotaxial growth of transition metal monopnictides remains to be developed.

A multi-technique study has been performed for the MBE growth of MnSb on $In_{0.48}Ga_{0.52}As$(111)A substrates, employing RHEED, AFM, SEM, STEM, EDX, XRD and VSM . A 3×3 grid of beam flux ratios $J_{Sb/Mn}$ and substrate temperatures T_{sub} has been studied. The flux ratio is critical and a balance must be struck between incorporating epitaxial Sb (high $J_{Sb/Mn}$) and allowing the exchange of metal species (mid $J_{Sb/Mn}$), while growth in Mn-rich conditions (low $J_{Sb/Mn}$) causes heavy disruption of the substrate with endotaxial MnAs growth and poor MnSb films. At $J_{Sb/Mn} = 6.5$ the optimum substrate temperature for growth appears to be lower than that used for growth on GaAs. In particular, interface sharpness is best at around $T_{sub} = 350$°C while surface smoothness is best at around $T_{sub} = 415$°C, and the coercive field improves when dropping from 415°C to 350°C. This suggests an overall optimum growth temperature between the two, i.e. rather lower than for growth on GaAs(111), but even at such a temperature it is not clear that both sharp interfaces and smooth, Sb inclusion-free films would be grown.

A simple two-stage growth method was employed to try to balance interface and surface smoothness, growing 2 nm of material at low $T_{sub} = 350°C$ before interrupting growth and raising to $T_{sub} = 415°C$. This reduced the density of surface crystallites, which were observed for all growth conditions, ranging in size between 0.1μm and 1μm. Furthermore the endotaxial growth of MnAs at low flux ratio was suppressed. However, the segregation of In and Ga from the substrate was not fully inhibited at the optimum flux ratio, which suggests that the MnSb overlayer is still incomplete at this stage (i.e. the morphology comprises disconnected islands). Hence a longer low-temperature growth stage and/or a growth interrupt may be useful, in order to allow the thin MnSb layer to fully cover the substrate and suppress In and Ga segregation. The growth interrupt itself may also be beneficial independently of the change of T_{sub}. It should be noted that the electrical properties of semimetallic MnSb should not be degraded by adsorption of a small fraction of a monolayer of contaminants, as might occur with a doped semiconductor material undergoing a long growth interrupt.

The goals of MBE growth optimization depend on the device structures targeted. For spin transport applications, the quality of the semiconductor/ferromagnet interface is generally thought to be most important. For a typical lateral spin valve structure, since metal contacts would subsequently be formed on the MnSb pads, its surface smoothness is not critical. Furthermore, in the present study the Sb inclusions do not appear to contact the interface where they would provide a non-spin polarized parallel conduction pathway. Finally a significant size or shape anisotropy difference between contacts is often used to allow switching of a single contact by an external field, and in such a case slightly non-optimal magnetic response may be tolerated. These considerations point towards lower MnSb growth temperatures. For applications where the magnetic saturation, coercivity and anisotropy of the MnSb films is more important, such as waveguide optical isolators [12] or micromagnetic structures, a poorer interface may be tolerated. This work suggests that further MBE growth studies for MnSb growth on $In_xGa_{1-x}As$, where interfacial intermixing is a particular challenge, should move beyond substrate temperature/flux ratio optimization to consider longer low-temperature growth stages and/or a growth interrupt early into the MnSb layer growth with the aim of fully suppressing In and Ga segregation.

References

[1] H. Akinaga, H. Ohno, Semiconductor spintronics, IEEE TRANSACTIONS ON NANOTECHNOLOGY 1 (1) (2002) 19–31. doi:10.1109/TNANO.2002.1005423.

[2] P. J. Simmonds, S. N. Holmes, H. E. Beere, I. Farrer, F. Sfigakis, D. A. Ritchie, M. Pepper, Molecular beam epitaxy of high mobility $In_{0.75}Ga_{0.25}As$ for electron spin transport applications, Journal of Vacuum Science & Technology B: Microelectronics and Nanometer Structures 27 (4) (2009) 2066. doi:10.1116/1.3156736.
URL https://doi.org/10.1116/1.3156736

[3] H. Kosaka, A. Kiselev, F. Baron, K. W. Kim, E. Yablonovitch, Electron g-factor engineering in III-V semiconductors for quantum communications, Electronics Letters 37 (7) (2001) 464. doi:10.1049/el:20010314.
URL https://doi.org/10.1049/el:20010314

[4] M. TANAKA, J. HARBISON, T. SANDS, T. CHEEKS, V. KERAMIDAS, G. ROTHBERG, Molecular-beam epitaxy of MnAs thin-films on GaAs, JOURNAL OF VACUUM SCIENCE & TECHNOLOGY B 12 (2) (1994) 1091–1094, 13th North American Conference on Molecular-Beam Epitaxy, STANFORD UNIV, STANFORD, CA, SEP 13-15, 1993. doi:10.1116/1.587095.

[5] V. Kaganer, B. Jenichen, F. Schippan, W. Braun, L. Daweritz, K. Ploog, Strain-mediated phase coexistence in heteroepitaxial films, PHYSICAL REVIEW LETTERS 85 (2) (2000) 341–344. doi:10.1103/PhysRevLett.85.341.

[6] D. H. Mosca, F. Vidal, V. H. Etgens, Strain engineering of the magnetocaloric effect in MnAs epilayers, PHYSICAL REVIEW LETTERS 101 (12). doi:10.1103/PhysRevLett.101.125503.

[7] H. Akinaga, T. Manago, M. Shirai, Material design of half-metallic zinc-blende CrAs and the synthesis by molecular-beam epitaxy, JAPANESE JOURNAL OF APPLIED PHYSICS PART 2-LETTERS 39 (11B) (2000) L1118–L1120. doi:10.1143/JJAP.39.L1118.

[8] J. D. Aldous, C. W. Burrows, A. M. Sanchez, R. Beanland, I. Maskery, M. K. Bradley, M. d. S. Dias, J. B. Staunton, G. R. Bell, Cubic MnSb:

Epitaxial growth of a predicted room temperature half-metal, PHYSICAL REVIEW B 85 (6). doi:10.1103/PhysRevB.85.060403.

[9] H. Akinaga, S. Miyanishi, W. Van Roy, J. De Boeck, G. Borghs, Influence of GaAs (001) surface termination on the in-plane magnetic anisotropies of MnSb epitaxial films, APPLIED PHYSICS LETTERS 73 (22) (1998) 3285–3287. doi:10.1063/1.122746.

[10] K. Ono, M. Shuzo, M. Oshima, H. Akinaga, Ga segregation in MnSb epitaxial growth on GaAs(100) and (111)B substrates, PHYSICAL REVIEW B 64 (8). doi:10.1103/PhysRevB.64.085328.

[11] J. D. Aldous, et al., Growth and characterisation of NiSb(0001)/GaAs(111)B epitaxial films, JOURNAL OF CRYSTAL GROWTH 357 (2012) 1–8. doi:10.1016/j.jcrysgro.2012.07.010.

[12] T. Amemiya, Y. Ogawa, H. Shimizu, H. Munekata, Y. Nakano, Semiconductor waveguide optical isolator incorporating ferromagnetic epitaxial MnSb for high temperature operation, Applied Physics Express 1 (2008) 022002. doi:10.1143/apex.1.022002.
URL https://doi.org/10.1143/apex.1.022002

[13] M. E. Islam, M. Akabori, Growth and magnetic properties of MnAs/InAs hybrid structure on GaAs(111)B, JOURNAL OF CRYSTAL GROWTH 463 (2017) 86–89. doi:10.1016/j.jcrysgro.2017.02.009.

[14] M. E. Islam, M. Akabori, In-plane isotropic magnetic and electrical properties of MnAs/InAs/GaAs(111)B hybrid structure, PHYSICA B-CONDENSED MATTER 532 (2018) 95–98, 3rd International Symposium on Frontiers in Materials Science (FMS), Hanoi, VIETNAM, SEP 28-30, 2016. doi:10.1016/j.physb.2017.03.013.

[15] H. Oomae, S. Irizawa, Y. Jinbo, H. Toyota, T. Kambayashi, N. Uchitomi, Studies of zinc-blende type MnAs thin films grown on InP(001) substrates by XRD, JOURNAL OF CRYSTAL GROWTH 378 (2013) 410–414, 17th International Conference on Molecular Beam Epitaxy (MBE), Nara, JAPAN, SEP 23-28, 2012. doi:10.1016/j.jcrysgro.2012.12.095.

[16] G. R. Bell, C. W. Burrows, T. P. A. Hase, M. J. Ashwin, S. R. C. Mcmitchell, A. M. Sanchez, J. D. Aldous, Epitaxial growth of cubic MnSb on GaAs and InGaAs(111), SPIN 04 (04) (2014) 1440025.

doi:10.1142/s2010324714400256.
URL https://doi.org/10.1142/s2010324714400256

[17] C. W. Burrows, A. Dobbie, M. Myronov, T. P. A. Hase, S. B. Wilkins, M. Walker, J. J. Mudd, I. Maskery, M. R. Lees, C. F. McConville, D. R. Leadley, G. R. Bell, Heteroepitaxial growth of ferromagnetic MnSb(0001) films on Ge/Si(111) virtual substrates, Crystal Growth & Design 13 (11) (2013) 4923–4929. doi:10.1021/cg4011136.
URL https://doi.org/10.1021/cg4011136

[18] K. Lawniczak-Jablonska, A. Wolska, M. T. Klepka, S. Kret, J. Gosk, A. Twardowski, D. Wasik, A. Kwiatkowski, B. Kurowska, B. J. Kowalski, J. Sadowski, Magnetic properties of MnSb inclusions formed in GaSb matrix directly during molecular beam epitaxial growth, Journal of Applied Physics 109 (7) (2011) 074308. doi:10.1063/1.3562171.
URL https://doi.org/10.1063/1.3562171

[19] N. Nishizawa, H. Munekata, Thickness dependence of magnetic anisotropy in MnSb epitaxial layers, Journal of Crystal Growth 378 (2013) 418–421. doi:10.1016/j.jcrysgro.2012.11.040.
URL https://doi.org/10.1016/j.jcrysgro.2012.11.040

[20] N. Liu, G. Gao, J. Liu, K. Yao, Preserving the half-metallicity at the interfaces of zinc-blende MnSb/GaSb heterojunction: A density functional theory study, Computational Materials Science 95 (2014) 557–562. doi:10.1016/j.commatsci.2014.08.026.
URL https://doi.org/10.1016/j.commatsci.2014.08.026

[21] C. E. Ouserigha, H. Wang, C. W. Burrows, G. R. Bell, Enhanced Spin Polarization at n-MnSb(0001)/InP(111) Interface, in: 2016 COMPOUND SEMICONDUCTOR WEEK (CSW) INCLUDES 28TH INTERNATIONAL CONFERENCE ON INDIUM PHOSPHIDE & RELATED MATERIALS (IPRM) & 43RD INTERNATIONAL SYMPOSIUM ON COMPOUND SEMICONDUCTORS (ISCS), 2016.

[22] G. Schmidt, D. Ferrand, L. Molenkamp, A. Filip, B. van Wees, Fundamental obstacle for electrical spin injection from a ferromagnetic metal into a diffusive semiconductor, PHYSICAL REVIEW B 62 (8) (2000) R4790–R4793. doi:10.1103/PhysRevB.62.R4790.

[23] G. Bell, C. McConville, T. Jones, Plasmon excitations and the effects of surface preparation in n-type InAs(001) studied by electron energy loss spectroscopy, APPLIED SURFACE SCIENCE 104 (1996) 17–23, 5th International Conference on Formation of Semiconductor Interfaces (ICFSI-5), PRINCETON, NJ, JUN 26-30, 1995. doi:10.1016/S0169-4332(96)00115-8.

[24] S. A. Hatfield, G. R. Bell, Growth by molecular beam epitaxy and interfacial reactivity of MnSb on InP(001), JOURNAL OF CRYSTAL GROWTH 296 (2) (2006) 165–173. doi:10.1016/j.jcrysgro.2006.08.031.

[25] K. W. Haberern, M. D. Pashley, GaAs(111)A-(2x2) reconstruction studied by scanning tunneling microscopy, Physical Review B 41 (5) (1990) 3226–3229. doi:10.1103/physrevb.41.3226.
URL https://doi.org/10.1103/physrevb.41.3226

[26] L. O. Olsson, L. Ilver, J. Kanski, P. O. Nilsson, C. B. M. Andersson, U. O. Karlsson, M. C. Håkansson, Core level and valence-band studies of the (111)2x2 surfaces of InSb and InAs, Physical Review B 53 (8) (1996) 4734–4740. doi:10.1103/physrevb.53.4734.
URL https://doi.org/10.1103/physrevb.53.4734

[27] S. Hatfield, G. Bell, Mapping the surface reconstructions of MnSb(0001) and (1-101), Surface Science 601 (23) (2007) 5368–5377. doi:10.1016/j.susc.2007.09.002.
URL https://doi.org/10.1016/j.susc.2007.09.002

[28] C. W. Burrows, T. P. A. Hase, M. J. Ashwin, P. J. Mousley, G. R. Bell, Depth sensitive x-ray diffraction as a probe of buried half-metallic inclusions, physica status solidi (b) 254 (2) (2016) 1600543. doi:10.1002/pssb.201600543.
URL https://doi.org/10.1002/pssb.201600543

[29] N. Nateghi, D. Menard, R. A. Masut, Large interface diffusion in endotaxial growth of MnP films on GaP substrates, JOURNAL OF APPLIED PHYSICS 116 (13). doi:10.1063/1.4896910.

[30] W. Braun, A. Trampert, V. M. Kaganer, B. Jenichen, D. K. Satapathy, K. H. Ploog, Endotaxy of MnSb into GaSb, JOURNAL OF CRYSTAL

GROWTH 301 (2007) 50–53, 14th International Conference on Molecular Beam Epitaxy (MBE XIV), Waseda Univ, Tokyo, JAPAN, SEP 03-08, 2006. doi:10.1016/j.jcrysgro.2006.09.022.

[31] T. Okita, Y. Makino, Crystal magnetic anisotropy and magnetization of MnSb, Journal of the Physical Society of Japan 25 (1) (1968) 120–124. doi:10.1143/jpsj.25.120.
URL https://doi.org/10.1143/jpsj.25.120

[32] F. de Boer, R. Boom, A. Miedema, Enthalpies of formation of liquid and solid binary alloys based on 3d metals: II alloys of chromium and manganese, Physica B+C 113 (1) (1982) 18 – 41. doi:https://doi.org/10.1016/0378-4363(82)90107-3.
URL http://www.sciencedirect.com/science/article/pii/0378436382901073

[33] K. Yamaguchi, Y. Takeda, K. Kameda, K. Itagaki, Measurements of heat of formation of GaP, InP, GaAs, InAs, GaSb and InSb, Materials Transactions, JIM 35 (9) (1994) 596–602. doi:10.2320/matertrans1989.35.596.
URL https://doi.org/10.2320/matertrans1989.35.596

[34] C. W. Burrows, S. A. Hatfield, F. Bastiman, G. R. Bell, Interaction of Mn with GaAs and InSb: incorporation, surface reconstruction and nano-cluster formation, Journal of Physics: Condensed Matter 26 (39) (2014) 395006.
URL http://stacks.iop.org/0953-8984/26/i=39/a=395006